Distinct phases within large RNP granules of *C. elegans* oocytes are associated with differential stress responses of RNA binding proteins

Brooklynne Watkins[1,2,*], Mohamed T. Elaswad[1,2,*], Chloe Pestrue[2], Katherine Sharp[2,3], Elizabeth Breton[2], Jennifer Schisa[1,2,#]

1. Central Michigan University, Biochemistry, Cell and Molecular Biology Program
2. Central Michigan University, Department of Biology
3. Current address: Department of Biology, University of Pittsburgh

*Equal contribution
Correspondence: schis1j@cmich.edu

ABSTRACT

One emerging paradigm of cellular organization of RNA and RNA binding proteins is the formation of membraneless organelles (MLOs). Examples of MLOs include several types of RNP (ribonucleoprotein) granules that form via phase separation. Proper regulation of the phase transitions of RNA binding proteins is critical as dysregulation can lead to disease states. Germ granules are small RNP granules conserved across metazoa. In *C. elegans,* when oogenesis undergoes an extended meiotic arrest, germ granules assemble into much larger, more complex RNP granules whose hypothesized function is to regulate RNA metabolism and maintain oocyte quality. As a step towards gaining insight into the function of RNP granules, in this report we characterize distinct phases for four RNA binding proteins in arrested oocytes. We find that PGL-1 is dynamic and has liquid-like properties, while MEG-3 has gel-like properties, both similar to their properties in small germ granules of embryos. We also show that MEX-3 exhibits gel-like properties in many regards but is more dynamic than MEG-3. We find CGH-1 is dynamic but does not consistently behave liquid-like, and may be an intermediate phase within RNP granules. We also show that the distinct phases of the RNA binding proteins are associated with differential responses to stress.

INTRODUCTION

Phase separation is an emerging principle of cellular organization. Among the well-studied membraneless organelles that assemble via liquid-liquid phase separation are ribonucleoprotein (RNP) granules composed of mRNA and RNA binding proteins. RNP granules include processing bodies (P-bodies) and stress granules in an array of

cell types, and germ granules in the germ line (Corbet and Parker 2019). Many RNA binding proteins in RNP granules can undergo reversible phase transitions among diffuse, liquid, and gel-like phases. Transitions among these phases can function as an adaptation to environmental and intracellular changes, and regulate mRNA metabolism (Alberti and Carra 2018). We know that proper regulation of phase transitions is critical because dysregulation can result in disease states. For example, in ALS mutations FUS phase separates into neuronal granules, and ectopic aggregates of FMRpolyG protein in ovarian stromal cells are associated with Fragile-X-associated primary ovarian insufficiency (Ganion 1991; Buijsen et al. 2016; Friedman-Gohas et al. 2020). While a growing number of *in vivo* studies have been building on *in vitro* observations that demonstrate a role for multivalent interactions in driving the condensation and decondensation of proteins, the precise regulation and function of phase transitions in oogenesis is not well understood.

Germ granules are evolutionarily conserved in germ lines across metazoa. They are essential for germ cell differentiation and fertility, and germ granules appear to be the site where small RNA pathways monitor germ line transcripts (Kawasaki et al. 2004; Spike et al. 2008; Billi et al. 2012; Pek et al. 2012; Updike et al. 2014; Trcek and Lehmann 2019; Sundby et al. 2021). Due to their more complex *in vivo* environment, germ granules differ from *in vitro* condensates that are simple, single-phase liquid droplets. *Drosophila* germ granules (polar granules) contain multiple homotypic clusters of RNAs within protein-rich condensates (Little et al. 2015; Trcek et al. 2015). Similarly, in zebrafish and *Xenopus* an amyloid-like scaffold organizes RNAs into specific subregions within germ granules (Boke et al. 2016; Fuentes et al. 2018; Roovers et al.

2018). In the early *C. elegans* embryo, germ granules (P granules) also have multiple phases. The intrinsically disordered protein MEG-3 is concentrated at the periphery of granules, while the RGG-domain protein PGL-3 is observed in the central core of granules (Wang et al. 2014; Putnam et al. 2019). Moreover, the MEG-3 phase has gel-like properties in terms of its dynamics and stability, whereas PGL-1 and PGL-3 are liquid-like, including a sensitivity to temperature change (Hanazawa et al. 2011; Wang et al. 2014; Saha et al. 2016; Putnam et al. 2019). Thus, it is well established that germ granules have a complex structure under physiological conditions; however, less is known about the larger RNP granules that assemble during certain stress conditions and extended meiotic arrest (Schisa et al. 2001; Jud et al. 2008; Snee and Macdonald 2009; Shimada et al. 2011).

The *Caenorhabditis* germ line provides an excellent model to study questions of RNA binding protein condensation (Schisa et al. 2001; Jud et al. 2008; Snee and Macdonald 2009; Shimada et al. 2011). In a young *C. elegans* hermaphrodite, oocytes undergo meiotic maturation every 23 minutes; however, within a few days of adulthood, the sperm become depleted, and meiosis arrests (McCarter et al. 1999a). In the arrested oocytes, several RNA binding proteins condense into large RNP granules that are up to 20 times larger than a typical cytoplasmic P granule in oocytes (Schisa et al. 2001). The condensation is reversible if sperm are resupplied via mating, or major sperm protein is injected (Schisa et al. 2001; Jud et al. 2008). Several mRNAs and diverse types of RNA binding proteins are detected in the large RNP granules including P-granule proteins, P-body proteins, stress granule proteins, and other RNA binding proteins associated with translational regulation such as the KH-domain protein MEX-3

(Jud et al. 2008; Noble et al. 2008; Hubstenberger et al. 2013). Based on their composition, the large RNP granules are hypothesized to regulate mRNA metabolism during extended delays in the fertilization of oocytes. In prior studies, laser-scanning confocal images of fixed worms hinted at substructure within the large RNP granules. For example, small foci of DCAP-1 appear to be docked on larger, heterogeneous granules of PAB-1 (Jud et al. 2008). However, distinct phases have not been identified within the granules.

In this study, we first uncover an imaging stress that differentially modulates the condensation of RNA binding proteins in oocytes. While PGL-1 and GLH-1 decondense in response to imaging stress, MEX-3, CGH-1, and CAR-1 condense into granules. This differential stress response prompted an analysis of the properties of PGL-1, CGH-1, MEX-3, and MEG-3 to determine if the phases of proteins change when very large granules assemble, and to determine if the large RNP granules in meiotically arrested oocytes have distinct phases. Similar to their phases in small P granules of early embryos, we find that PGL-1 has liquid-like properties, and MEG-3 has gel-like properties. MEX-3 and CGH-1 may be intermediate phases, as they are insensitive to heat, like MEG-3, but CGH-1 appears fairly mobile via FRAP analyses, like PGL-1. We conclude the large RNP granules in arrested oocytes have distinct phases, and the phases correspond to the differential stress responses of RNA binding proteins.

METHODS

Strains and maintenance

All worms were grown on nematode growth media using standard conditions at 20°C (Brenner 1974) unless specified. Strains used include: DG4269 mex-

3(tn1753[gfp::3xflag::mex3]), OD61 ltIs41[pAA5; pie-1::GFP-TEV-Stag::CAR-1; unc-119(+)], JH3644 *fog-2(g71)* V; meg-3(ax4320)[meg-3::mCherry)]X, CL2070 dvIs70 [hsp-16.2::GFP + rol-6(su1006)], SJ4005 zcIs4 [hsp-4::GFP] V, LD1171 ldIs4 [gcs-1p::GFP + rol-6(su1006)], OH16024 daf-16(ot971[daf-16::GFP]), JH3269 pgl-1(ax3122[pgl-1::gfp]), DUP64 *glh-1(sam24[glh-1::GFP::3xFLAG])*, JH1985 *unc-119(ed3); axIs1436[pCG33* pie-1prom:LAP::CGH-1]. Some strains were crossed into CB4108 *fog-2(q71)* as noted. Worms were synchronized using the hypochlorite bleach method.

Microscopy and Image analysis

Worms were picked onto slides made with 2% agarose pads and paralyzed using 6.25mM levamisole. To image diakinesis oocytes of young hermaphrodites, synchronized 1 day post-L4-stage worms were used. To image meiotically arrested oocytes in *fog-2* strains, L4 females were separated from males and imaged 1 or 2dpL4 as indicated in figure legends.

Images were collected within 15 minutes of slide preparation unless otherwise noted. Imaging was done using a Leica compound fluorescence microscope (low magnification images of whole worms in Fig.S1) or a Nikon A1R laser scanning confocal microscope (all other images). All images for a given strain were collected using identical levels and settings. The number of granules in oocytes and total integrated density (intensity of fluorescence in granules) was determined using ImageJ particle analysis. In Figure 4, the threshold to categorize dispersed PGL-1 was determined by the lowest fluorescence intensity in granules seen in the control 0-10 min. worms. The threshold for condensed CAR-1 was determined to be >3x higher intensity than in control 0-10 min. worms.

Imaging using oxidative stress and ER stress reporters

The positive control for *gcs-1*::GFP was incubating young adults at 34°C for 3.5 hrs and recovering at 20°C for 1 hr before imaging (An and Blackwell 2003). The positive control for *hsp-16.2*::GFP was 34°C for 2 hrs and recovering at 20°C for 12 hr before imaging (Strayer et al. 2003). The positive control for *hsp*-4::GFP was 8 hours at 30°C before imaging (Bischof et al. 2008). Controls were compared to worms imaged within <25 min. or 60-90 min. after being prepared. GFP levels in images were qualitatively scored using scorecards.

Heat stress

The Tokai Hit stage top incubator was used at 34°C with the Nikon A1R laser scanning confocal microscope. Worms were placed on small NGM plates and incubated at 34°C in the stage top incubator for 40 minutes, or 2 hours as noted, before being transferred to a slide and imaged at 34°C within 15 minutes.

Hexanediol assays

The hexanediol protocol of Updike et al., was adapted (2011). Worms were individually picked into 1 µL of egg buffer (25 mM Hepes, 120 mM $NaCl_2$, 2 mM $MgCl_2$, 2 mM $CaCl_2$, and 48 mM KCl_2) on a poly-L-lysine coated coverslip. The worm was dissected at both the proximal and distal end to release the gonad arms. Worms were imaged using the 60x objective every 2 seconds. After collecting baseline images (pre-treatment), 1ul of either egg buffer, 10% 1,6-hexanediol, or 1.0% SDS was added, and images were collected for 60 seconds (post-treatment). ImageJ was used to quantitate the number of granules and granule intensity in oocytes of pre- and post-treatment images. The ratio of pre/post values was graphed to determine if granules dissolved.

Fluorescence Recovery After Photobleaching

For all strains, the 488 laser was used to photo-bleach an area of 3.68 μm^2 within a single RNP granule in a -2 to -6 oocyte of a *fog-2* female. All proteins were imaged using a 500ms exposure and a 60x objective. Images were acquired every 8s during a recovery phase of 300s after photobleaching. The fluorescence intensities were normalized by dividing the intensity of the bleached zone by an unbleached fluorescent area (Hubstenberger et al. 2013). ImageJ was used to correct for movements during imaging. The Stacks-Shuffling-MultiStackReg plugin was used to align time series to an image at t=0.

Statistical analysis

Sample sizes were determined using G*Power 3.1 for power analyses; all experiments were blinded and done at least in triplicate. Data are presented as mean $\pm$ SEM unless otherwise indicated. Statistical analyses were performed on GraphPad Prism 9.1, and specific tests are noted in figure legends. P-values <0.05 were considered statistically significant.

Data Availability

All strains are available at the *Caenorhabditis* Genetics Center (CGC) or on request from the Schisa lab or other *C. elegans* labs. The authors affirm that all data necessary to confirm the conclusions in this article are included in the article, figures, and tables.

RESULTS AND DISCUSSION

Imaging conditions can inadvertently induce stress and phase transitions

The regulation of RNA binding protein phase transitions in the germ line is not well understood. While investigating candidate regulators of the RGG domain-protein PGL-1 in the adult germ line, we noticed unanticipated dispersal of PGL-1 during imaging of control RNAi-treated worms. Early in the imaging session, PGL-1 was detected in punctate P granules throughout the adult germ line as expected (Strome and Wood 1982); however, over extended time (late), PGL-1 became dispersed in oocytes and the distal core, appearing at increased levels throughout the cytosol and decreased levels in punctate granules (Fig. 1A). To determine if our imaging conditions were inadvertently inducing a stress response, we used the DAF-16::GFP strain (Aghayeva et al. 2020). The DAF-16 FOXO (forkhead box class O) transcription factor translocates from the cytoplasm to the nucleus in response to unfavorable conditions such as heat stress, oxidative stress, starvation, or when cellular repair is needed (Oh et al. 2005; Henderson et al. 2006). We categorized the subcellular localization of DAF-16 as cytoplasmic, nuclear, or intermediate (mix of cytoplasmic and nuclear) (Oh et al. 2005). We found that DAF-16 was mostly cytoplasmic or intermediate in worms imaged within 25 minutes of slides being prepared (worms picked into 6.25 mM levamisole on a 2% agarose pad and coverslip added); only 7% were scored as nuclear (Fig. 1B,C). For the purpose of a contrasting experiment, we chose a much later time range of imaging 60-90 minutes after slides were prepared. In contrast to the early-imaged worms, 73% of worms that were scored late during imaging had nuclear localization of DAF-16, and

none were cytosolic. Based on these results, we consider late-imaging conditions as imaging stress.

Levamisole is a paralytic agent frequently used as an anesthetic to mount worms for imaging. While one study showed that DAF-16 remains cytoplasmic after worms are exposed to 1mm levamisole and recovered for 30 minutes (Manjarrez and Mailler 2020), exposure to levamisole can affect autophagy and result in increased numbers of GFP::LGG-1 puncta in somatic cells (Zhang et al. 2015). We therefore asked if exposure to levamisole is sufficient to induce PGL-1 decondensation or DAF-16 translocation. We incubated PGL-1::GFP worms in 50 μl of 6.25mM levamisole for 15 or 60 min in a humidity chamber prior to placing them on an agarose pad and imaging within 15 minutes. We observed punctate PGL-1 granules in both samples, with no sign of the dispersed PGL-1 observed in late-imaged worms (Fig. 1A). In a large majority of worms incubated a short time in levamisole we observed cytoplasmic DAF-16::GFP, with only 18% having an intermediate phenotype of partial nuclear translocation (Fig. 1B,C). In contrast, 63% of worms incubated an extended amount of time in levamisole had intermediate DAF-16 translocation, and in 5% of worms DAF-16 was nuclear. Because the ‘extended levamisole’ worms exhibited a weaker DAF-16 stress response than the late-imaged worms, we conclude levamisole is not the main source of stress during imaging. Our results suggest that while levamisole can contribute to a mild DAF-16 stress response, additional aspects of extended imaging are more critical to induce decondensation of PGL-1 granules.

RNA binding proteins are differentially sensitive to imaging stress

To determine the extent to which imaging stress affects phase transitions of RNA binding proteins, we first quantitated the effects on two P-granule proteins using the same conditions as for DAF-16. As expected for PGL-1, given our initial observations during RNAi experiments (Fig. 1), we observed significantly fewer granules of GFP::PGL-1 in oocytes and fewer granules in the distal nuclei, late during imaging (Fig. 2A,B). We also observed significant decondensation of GFP::GLH-1 in oocytes and the distal nuclei although the dispersal of protein out of granules was not as penetrant as with PGL-1 (Fig. 2A,B). We conclude imaging stress can induce the decondensation of multiple P-granule proteins.

We next asked if imaging stress affects three RNA binding proteins that are normally dispersed throughout oocytes. MEX-3 is a KH-domain protein that localizes to P granules in embryos, but is mostly diffuse throughout the cytosol of oocytes (Draper et al. 1996). In response to imaging stress the majority of the GFP::MEX-3 protein appeared to remain decondensed throughout the cytoplasm; however, we detected a variable but significant increase in the number of small GFP::MEX-3 granules in oocytes (Fig. C,D). CGH-1 and CAR-1 are orthologs of the P-body proteins Me31B/RCK and Trailerhitch/RAP55/Lsm14 (Schisa 2012). Both proteins localize to P granules and throughout the cytosol of oocytes (Navarro et al. 2001; Boag et al. 2005). After imaging stress, the number of GFP::CGH-1 granules was variably increased; in a minority of worms, more than 7 times as many granules were detected compared to the control (Fig. 2C,D). Imaging stress also resulted in increased numbers of GFP::CAR-1 granules that were enriched at the nuclear envelope, as well as enriched along the cortical

membrane (Fig. 2C,D). We also observed enrichment at the cortex in a subset of control and stressed worms (Fig. 1C arrowhead). Overall, we conclude the response of RNA binding proteins to imaging stress varies. MEX-3, CGH-1, and CAR-1 condense into granules, opposite of the decondensation observed for PGL-1 and GLH-1.

When *C. elegans* hermaphrodites run out of sperm after 3-4 days of adulthood, or lack sperm due to a feminizing mutation such as *fog-2*, meiotic arrest is extended, and large ribonucleoprotein (RNP) granules assemble in oocytes (McCarter et al. 1999b; Schisa et al. 2001). The large RNP granules can be up to 20 times the size of a typical cytoplasmic P granule in oocytes, and are considered hybrid granules as they are condensates comprised of P-granule proteins, P-body proteins, stress granule proteins, and other RNA binding proteins (Schisa et al. 2001; Schisa 2019). The dynamics of proteins can decrease as granules increase in size (Hubstenberger et al. 2013). Moreover, the properties and functions of RNA binding proteins can be disrupted upon phase transitions. For example, in *Drosophila* egg chambers in the absence of the E3 ubiquitin ligase HECW, the Me31B RNA binding protein transitions from small granules in a liquid phase to larger granules in a gel-like phase, and translational repression of target mRNAs is deregulated (Fajner et al. 2021). Since slower dynamics and increased stability can occur as RNP granules increase in size, we asked if imaging stress affects the condensation of four RNA binding proteins in the large RNP granules of meiotically arrested oocytes. In early-imaged oocytes, we observed large granules of GFP::MEX-3 and GFP::CGH-1 as expected (Schisa et al. 2001; Jud et al. 2008; Noble et al. 2008). After imaging stress, we did not detect any significant changes in the number of granules or the intensity of GFP fluorescence in granules, suggesting no

major change in condensation (Fig. 3A,B). Therefore, within the large granules of arrested oocytes MEX-3 and CGH-1 appear to be more stable and less sensitive to imaging stress than in diakinesis oocytes (Fig. 2C). In contrast, PGL-1 granules were reduced in number and intensity after imaging stress, compared to the control where a heterogeneous mix of small and very large, bright granules were detected as expected (Fig. 3A,B; (Jud et al. 2008; Noble et al. 2008)). Thus, we conclude imaging stress induces decondensation of large PGL-1 aggregates in arrested oocytes, similar to its effect on the small P granules in oocytes of young hermaphrodites. Lastly, we examined the effect of imaging stress on MEG-3. MEG-3 is normally detected at low levels in oocytes and strongly localizes to P granules in embryos (Wang et al. 2014). During extended meiotic arrest MEG-3 underwent a dramatic phase transition and condensed into large granules as previously reported (Putnam et al. 2019). We detected no significant changes in granule number or intensity after extended imaging (Fig. 3A,B). Overall, these data suggest the MEX-3, CGH-1, and MEG-3 proteins within large RNP granules of arrested oocytes may be less liquid-like phases than PGL-1.

Imaging conditions can induce a rapid stress response

Having established that imaging stress can inadvertently trigger either condensation or decondensation of RNA binding proteins, we next asked how quickly the stress occurs while imaging. We first examined DAF-16::GFP worms that were prepared prior to imaging for a maximum of 10, 20, or 30 minutes. In the majority of 0-10-minute worms, DAF-16 was cytoplasmic, and none had strong nuclear localization (Fig. 4A,B). In contrast, after 11-20 minutes, DAF-16 was nuclear in 69% of worms and intermediate in

the remaining 31% of worms (Fig. 4A,B). In the 21-30 min. worms, DAF-16 was nuclear in >80% of worms. These time course data indicate that some level of stress occurs within 11-20 minutes of worms being prepared for imaging, and is relevant for all researchers using imaging methods to consider.

We next asked if the RNA binding protein phase transitions are induced as quickly as DAF-16 nuclear translocation. We first examined PGL-1, and noted that in 30% of 11-20 min. worms, PGL-1 was at least partially dispersed, compared to the 0-10 min. worms which had bright PGL-1 granules as expected (Fig. 4B). We categorized PGL-1 as dispersed when the PGL-1 intensity in granules was below the lowest intensity observed in the 0-10 min. worms (see methods). The decondensation of PGL-1 was quite variable at all time points, and not statistically significant until the 51-60-min. worms; however, it was clear that at least modest decondensation can occur in some worms within the same time frame as DAF-16 translocation. We next assayed PGL-1 in arrested oocytes after 0-10 min. of imaging and observed a mix of small and large PGL-1 granules in cortical slices as expected (Fig. 4C). PGL-1 appeared dispersed in 17% of worms at 11-20 min.; however, within 21-30 min. of imaging, we observed a significant increase in the percentage of worms with dispersed PGL-1 (Fig. 4C). At longer time points, we continued to observe significant dispersal of PGL-1; however, the penetrance of the response was variable (Fig. 4C). Lastly, we examined the response of CAR-1. In the 0-10 min. worms CAR-1 was mostly diffuse throughout the cytoplasm as expected (Fig. 4D). After 11-20 min., CAR-1 condensation was observed in 40% of worms; condensation was defined as worms having >3x as many CAR-1 granules as the largest number of granules in 0-10 min. worms (Fig. 4D). We noted that many granules were

localized to the cortex; therefore, cortical slices were quantitated. At the three time points beyond 20 min., CAR-1 was condensed in 60-100% of worms (Fig. 4D). Based on these observations, we conclude that while imaging stress induces changes both to DAF-16 translocation and RNA binding protein condensation, the effects on RNA binding proteins are more variable. Nonetheless, inadvertent phase transitions can occur within 11-20 min. of imaging which is fairly rapid, especially if researchers routinely prepare their worms at a distant location from their microscopy facility.

Once we established a time course of imaging stress, we wanted to identify the type of stress induced by the imaging conditions. We used two reporter strains to ask if oxidative stress is induced: *gcs-1p*::gfp and *hsp-16.2*::gfp. GCS-1 (gamma-glutamyl-cysteine synthetase heavy gene) is a detoxification gene that is induced in the intestine in response to oxidative stress, including heat-induced increases in intracellular reactive oxygen species (ROS) (An and Blackwell 2003; Wang et al. 2010). HSP-16.2 is a small heat shock protein that is also induced by oxidative stress (Link et al. 1999). In the positive control *gcs-1p*::gfp worms, we observed moderate or high GFP expression in 100% of the worms (Fig. S1). In contrast, in worms imaged early during imaging without heat, moderate or high levels of expression were detected in only 4% of worms, and the GFP expression did not significantly increase after imaging stress (Fig. S1). In the positive control *hsp-16.2*::gfp worms, high expression was seen in 100% of worms. In contrast, low expression was observed in worms imaged both early and after imaging stress (Fig. S1). We also asked if ER stress is induced by using the *hsp-4*::gfp reporter. HSP-4 is the immunoglobulin heavy chain-binding protein (BiP) homolog, and a reporter for the unfolded protein response (UPR) that prepares cells for expansion of the ER

(Shen et al. 2001; Kapulkin et al. 2005; Walter and Ron 2011). In the positive control, after 8 hours of 30°C heat stress, we observed moderate or high GFP levels in 96% of worms as expected (Bischof et al. 2008). In contrast, 100% of worms imaged early had low levels, and 98% of worms maintained low levels after imaging stress (Fig. S1). Overall, these results suggest the oxidative, ER stress, and heat stress pathways are not stimulated at high levels by imaging stress, and a different type of stress is induced by extended imaging.

RNA binding proteins within large RNP granules exhibit distinct responses to elevated temperature

P granules in early embryos have multiple phases; PGL-1/-3 behave as liquid phases, and MEG- 3 is a gel-like phase (Putnam et al. 2019). One explanation for the opposite responses of PGL-1 and MEX-3/CGH-1 to imaging stress could be that PGL-1 is a liquid phase of the large RNP granules in arrested oocytes, and as such it decondenses, while MEX-3, CGH-1 and MEG-3 are less liquid-like. Sensitivity to temperature changes can help distinguish liquid phases from solid phases (Weber and Brangwynne 2012; Banani et al. 2017); therefore, we exposed *fog-2(q71)* females with arrested oocytes to 34°C and monitored the distribution of GFP in reporter strains. In control *fog-2*; GFP::PGL-1 females, large aggregates of PGL-1 granules were detected at the cortex among a heterogeneous mix of granules as expected (Jud et al. 2008) (Fig. 5A). In contrast, after 40 minutes at 34°C, while there was no statistical difference in overall numbers of granules, fewer large granules were apparent, and the total intensity of PGL-1 in individual granules was significantly reduced (Fig. 5B,C). In

diakinesis oocytes of young hermaphrodites, PGL-1 also decondenses after heat stress (Jud et al. 2008; Fritsch et al. 2021; Watkins and Schisa 2021). Therefore, we conclude PGL-1 granules are sensitive to increased temperature in both diakinesis and arrested oocytes, consistent with a liquid phase and similar to the behavior of PGL-1 in early embryos. We next asked if MEG-3 is sensitive to elevated temperature and assayed *fog-2*; mCherry::MEG-3 females. We observed large granules in arrested oocytes of both control and 34°C worms (Fig. 5A), and no significant changes in granule number or intensity were detected (Fig. 5B,C). Therefore, as in the embryo, MEG-3 seems stable at high temperatures in arrested oocytes, consistent with a gel-like phase.

To build on our imaging stress results, we next asked if CGH-1 is sensitive to elevated temperature by examining *fog-2*; GFP::CGH-1 females. After we did not observe a response to 40 minutes of heat stress, we assayed the oocytes after 2 hours at 34°C. We did not detect any changes qualitatively or any significant changes in the number of granules; however, the intensity of GFP::CGH-1 in granules decreased slightly (Fig. 5A-C). Compared to PGL-1, CGH-1 appears relatively stable in granules after an upshift in temperature. Lastly, we asked if MEX-3 is sensitive to temperature changes. In control *fog-2*; GFP::MEX-3 females we detected large granules enriched at the cortex of arrested oocytes as expected (Jud et al. 2008) (Fig. 5A). We did not observe a response to heat after 40 minutes, but after 2 hours at 34°C we observed a modest but significant increase in the number of granules, and increased intensity of MEX-3 in granules (Fig. 5B,C). We therefore also asked if MEX-3 responds to elevated temperature in diakinesis oocytes. In contrast to the modest change observed during the imaging stress (Fig. 2C,D), the majority of the MEX-3 protein that is normally

dispersed throughout the oocyte cytosol appeared condensed into granules at the cortex or nuclear envelope (Fig. 5A,B). This result is consistent with a prior heat stress experiment performed using anti-MEX-3 antibodies on fixed worms (Jud et al. 2008). We conclude MEX-3 responds strongly to increased temperature by undergoing condensation in diakinesis and arrested oocytes, possibly consistent with a gel-like phase. Taken together, all of the temperature shift experiments are consistent with the imaging stress data and identify PGL-1 as the most liquid-like protein in large RNP granules.

The PGL-1 phase within large oocyte RNP granules is liquid-like

To further characterize the phases of RNA binding proteins within large RNP granules, we next extruded gonads of *fog-2* females into the aliphatic alcohol, hexanediol, a chemical shown to dissolve liquid phases (Patel et al. 2007; Lin et al. 2016). Hexanediol (HD) disrupts hydrophobic interactions, and induces the dispersal of P granule proteins in diakinesis oocytes (Updike et al. 2011). We analyzed the data by plotting the ratio of granule number pre- and post-treatment, where no change would be 1.0. In egg buffer-treated control worms, we observed variable photobleaching in most worms, with a mean ratio of 0.54 (Fig. 6A,B). After exposing dissected gonads of *fog-2*; GFP::PGL-1 to 5% HD, we observed a variable response and a decreased mean ratio of 0.36. In 55% of HD-treated germ lines, we observed a significant reduction in granule number (defined as a pre/post ratio $\leq$ 0.27), compared to only 11% of the control germ lines (Figure 6A,B). This decrease in PGL-1 granule number in arrested oocytes suggests a

similar dispersal of PGL-1 within large RNP granules as that seen in the small P granules of diakinesis oocytes and embryos(Updike et al. 2011; Putnam et al. 2019).

We next exposed dissected gonads of *fog-2*; GFP::MEX-3 and *fog-2*; GFP::CGH-1 to HD. In both strains, the granules appeared fairly stable with no significant change in response to HD (Fig. 6C,D). However, the granules did not appear to be irreversible aggregates because they rapidly dissolved upon exposure to the detergent SDS (Fig. 6C,D). One caveat to the interpretation of HD experiments is that they are not direct measures of liquid phases. Recent *in vitro* reports reveal that at 5-10% concentrations of HD, kinases and phosphatases are inactive, and intermediate filaments dissolve, both of which could mask the properties of proteins (Lin et al. 2016; Duster et al. 2021). Nonetheless, these data are consistent with a liquid-like PGL-1 phase in RNP granules, and distinct phases of MEX-3 and CGH-1 that could be more gel-like.

RNP granule proteins within arrested oocytes exhibit distinct dynamics and occupy distinct phases

To determine RNA binding protein dynamics within RNP granules of arrested oocytes, we used fluorescence recovery after photobleaching (FRAP). We determined the rates of exchange within a large granule by photobleaching a 3.68μm^2 area in the center of a large granule. We found that PGL-1 and CGH-1 exhibited high rates of exchange (Fig. 6D). The rapid recovery for PGL-1 was similar to that observed for granule-to cytoplasm exchange in arrested oocytes (Putnam et al. 2019). In contrast, MEX-3 exhibited a lower rate of exchange but was still mobile. The moderate recovery of MEX-3 was not as complete as that seen for the CAR-1 RNA binding protein within RNP granules in

arrested oocytes (Hubstenberger et al. 2013). MEG-3 had extremely slow exchange dynamics, close to the absence of exchange that was previously reported for granule-to-cytoplasm exchange (Fig. 6D) (Putnam et al. 2019).

When we consider all of the data together, we conclude RNP granules of arrested oocytes have distinct phases (Table 1). All of the assays consistently show that PGL-1 is dynamic and a liquid-like phase of RNP granules. They also demonstrate that MEX-3 and MEG-3 are not as dynamic or liquid-like. MEG-3 has the slowest dynamics via FRAP, and MEX-3 showed the strongest condensation phenotypes at elevated temperature. Both proteins may be a gel-like phase of RNP granules, and one or both could act as scaffolding or otherwise promote the condensation of other RNA binding proteins into granules. The FRAP data for CGH-1 showed strongly dynamic behavior within large RNP granules. These data were somewhat surprising since CGH-1 was not sensitive to imaging stress, or strongly sensitive to elevated temperature or hexanediol treatment. CGH-1 may be an intermediate phase, distinct from PGL-1 and MEG-3. Ultimately, having a better understanding of the phases of RNP granules in arrested oocytes may lead to insights into the function of each condensed RNA binding protein when fertilization is delayed an extended time.

TABLE 1. Differential protein dynamics in large RNP granules suggest distinct phases.

	Oogenesis stage	PGL-1	CGH-1	MEX-3	MEG-3
Imaging stress	diakinesis	decondense	condense	condense	not tested
	arrested	decondense	stable	stable	stable
Temp. shift	arrested	decondense	partially decondense	condense	stable
Hexanediol	arrested	dissolve	stable	stable	not tested
SDS	arrested	not tested	dissolve	dissolve	not tested
Mobility (FRAP)	arrested	mobile	mobile	moderately mobile	less mobile

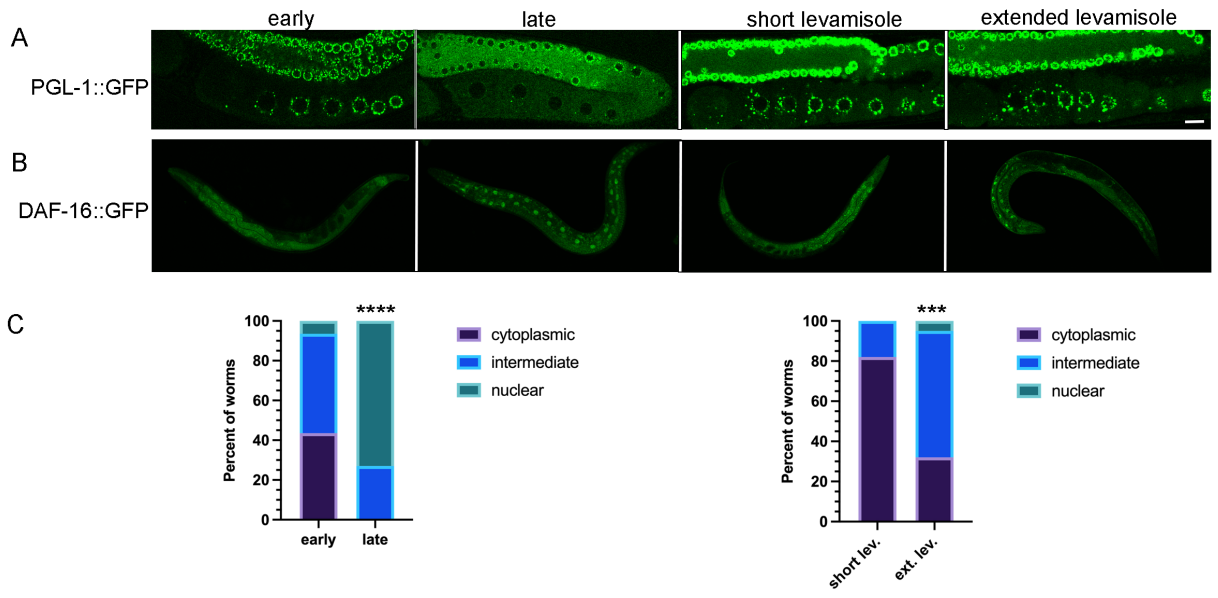

Figure 1. Imaging conditions can inadvertently induce stress. (A) Subcellular localization of PGL-1::GFP in the germ line: early during imaging process (within 25 min.) or after extended time imaging (60 min.); and after short (15 min.) or extended (60 min.) exposure to 6.25mM levamisole prior to mounting worms on a slide. Proximal oocytes are oriented on the bottom left in all images. Scale bar is 10 μm. (B) Subcellular localization of DAF-16::GFP in young hermaphrodites: imaging was done early (within 25 min.) or late (after 60-90 min.) of slides being prepared; and after short (15 min.) or extended (60 min.) exposure to 6.25mM levamisole. (C) Graphs show the percent of DAF-16::GFP worms with cytoplasmic distribution, intermediate distribution, or nuclear localization. Statistical significance was determined using the Fisher Exact Test. **** indicates $p<0.0001$; *** indicates $p<0.001$. n=15 (early), 16 (late), 28 (short), 19 (long).

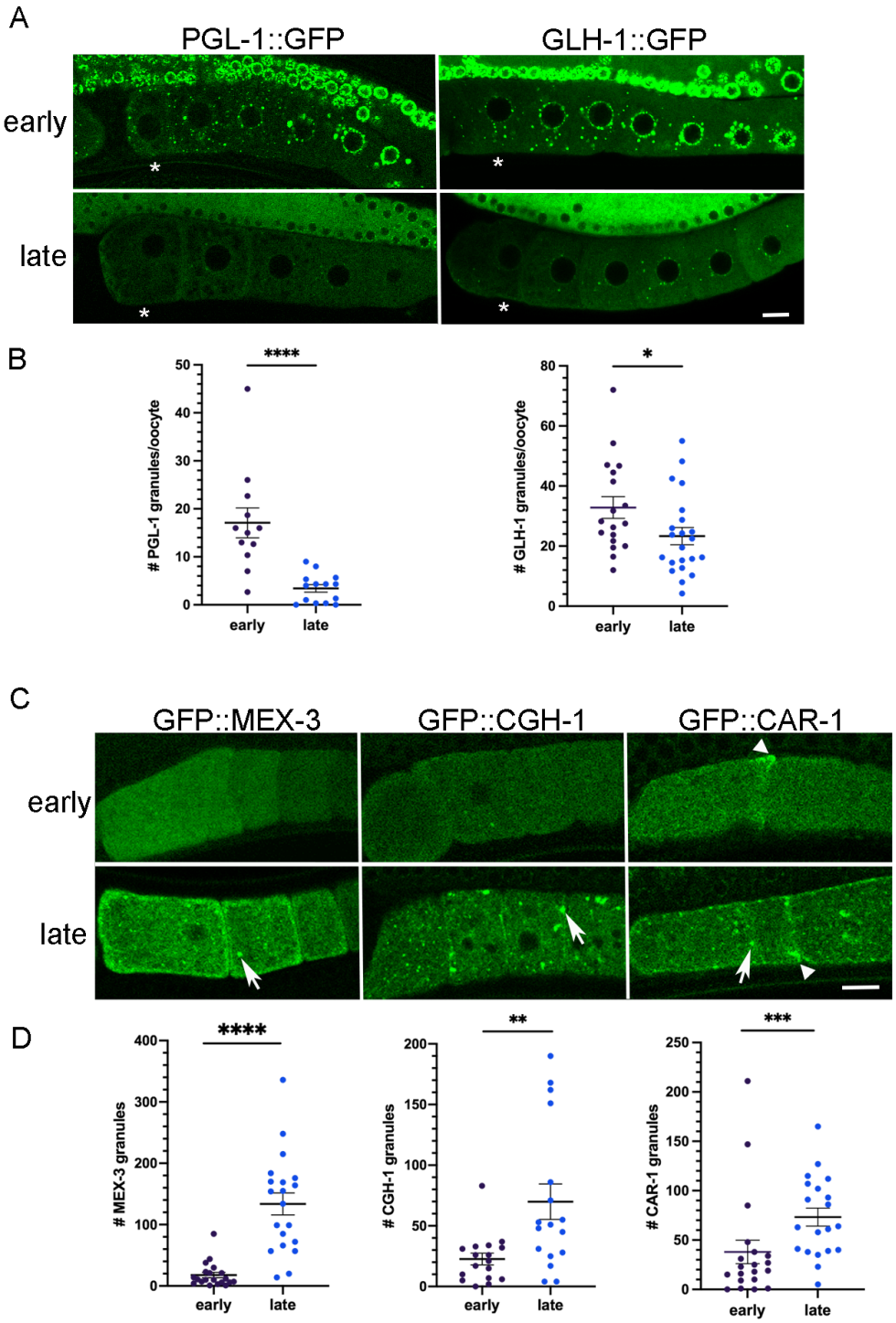
A
PGL-1::GFP
GLH-1::GFP
early
late
B
****
PGL-1 granules/oocyte
early
late
*
GLH-1 granules/oocyte
C
GFP::MEX-3
GFP::CGH-1
GFP::CAR-1
early
late
D
****
MEX-3 granules
**
CGH-1 granules
***
CAR-1 granules

Figure 2. RNA binding protein phase transitions are differentially sensitive to imaging stress. (A) Micrographs of GFP-tagged P granule protein reporter strains, PGL-1::GFP and GLH-1::GFP. Top row: Distribution of GFP in germ line early during imaging; Bottom row: Distribution of GFP in germ line after extended imaging (late) with strongest phenotypes shown. Asterisk marks the most proximal oocyte in each germ line. Smaller distal pachytene nuclei are visible at top of each image. Scale bar is 10 μm. (B) Graphs showing the number of GFP granules in a single Z-slice of proximal oocytes (see Methods). Statistical significance was determined using the Mann-Whitney test. **** indicates $p<0.0001$; * indicates $p<0.05$. n= 16-26. (C) Micrographs of GFP-tagged RNA binding protein reporter strains (MEX-3, CGH-1, and CAR-1) in most proximal oocytes. Top row: Distribution of GFP early during imaging; Bottom row: Distribution of GFP after extended imaging (late) with strongest phenotypes shown. Arrows indicate ectopic granules; arrowheads indicate cortical enrichment. Scale bar is 10 μm. (D) Graphs showing the number of GFP granules in a single Z-slice of proximal oocytes. Statistical significance was determined using the Mann-Whitney test. **** indicates $p<0.0001$, *** indicates $p<0.001$, ** indicates $p<0.01$. n=17-20. Error bars indicate mean ±SEM.

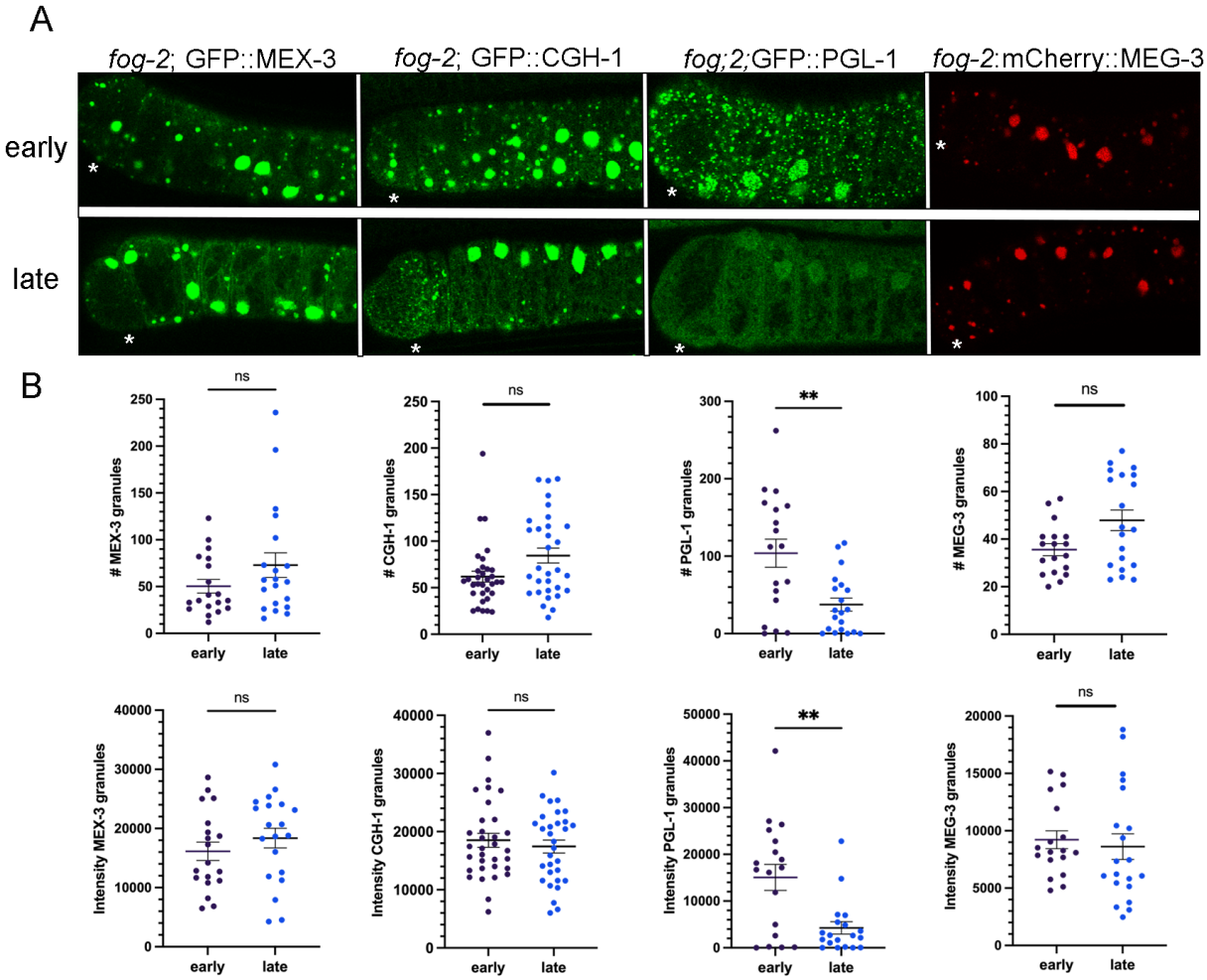

Figure 3. Imaging stress differentially affects RNA binding proteins in large RNP granules of meiotically arrested oocytes. (A) Micrographs of GFP-tagged RNA binding proteins (MEX-3, CGH-1, PGL-1, MEG-3) in a *fog-2* background. Top row: Distribution of GFP in arrested oocytes early during imaging. Bottom row: Distribution of GFP in arrested oocytes after extended imaging (late). Asterisk marks the most proximal oocyte in each germ line. Scale bar is 10 μm. (B) Graphs showing either the number of GFP granules or the integrated density of GFP in granules in a single Z-slice of proximal oocytes (see Methods). Statistical significance was determined using the Mann-Whitney test. ** indicates $p<0.01$, ns indicates not significant. n=18-33. Error bars indicate mean ±SEM.

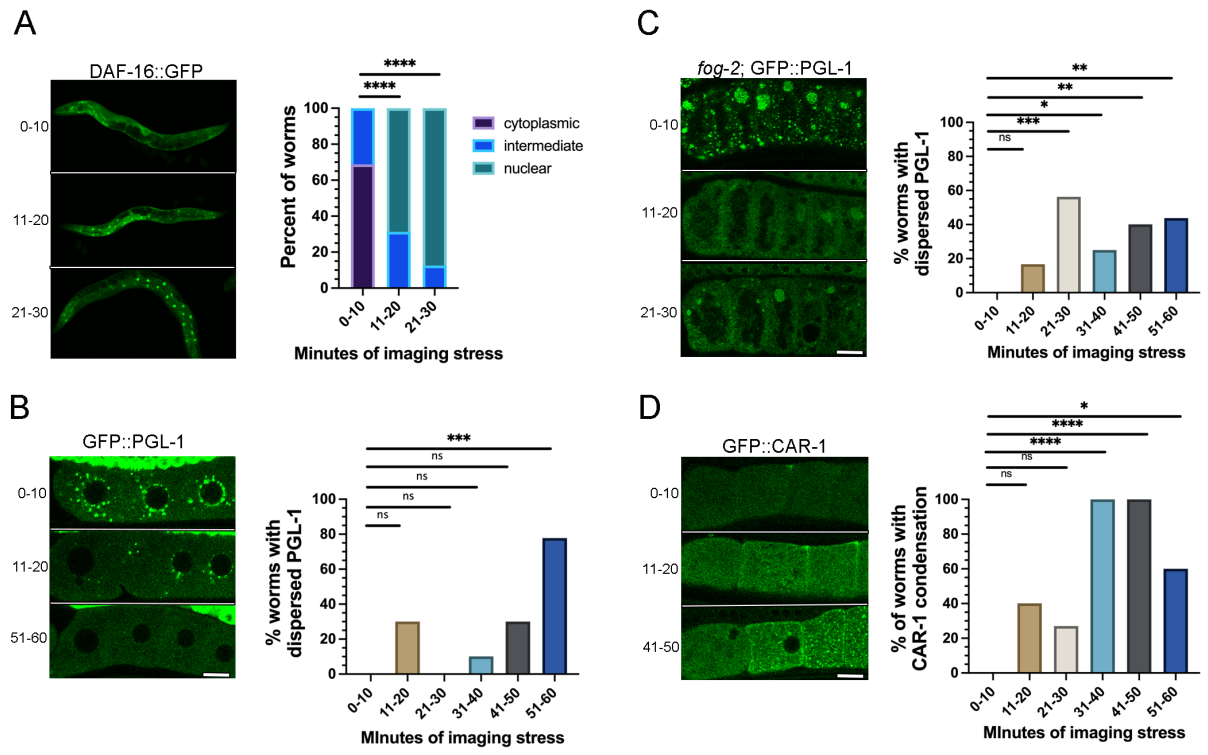

Figure 4. Imaging stress quickly triggers stress and affects phase transitions. (A-D) Time course of imaging stress effects on DAF-16, PGL-1, and CAR-1. For each reporter, micrographs of GFP-tagged strains are shown on the left with proximal oocytes oriented to the left, and graphs show the percent of worms with nuclear translocation (DAF-16) or phase transitions (PGL-1, CAR-1). All scale bars are 10 μm. See methods and text for description of thresholds used to categorize phase transitions. Statistical significance was determined using the Kruskal-Wallis test. **** indicates $p<0.0001$, *** indicates $p<0.001$, ** indicates $p<0.01$, * indicates $p<0.05$, ns indicates not significant. n=9-15.

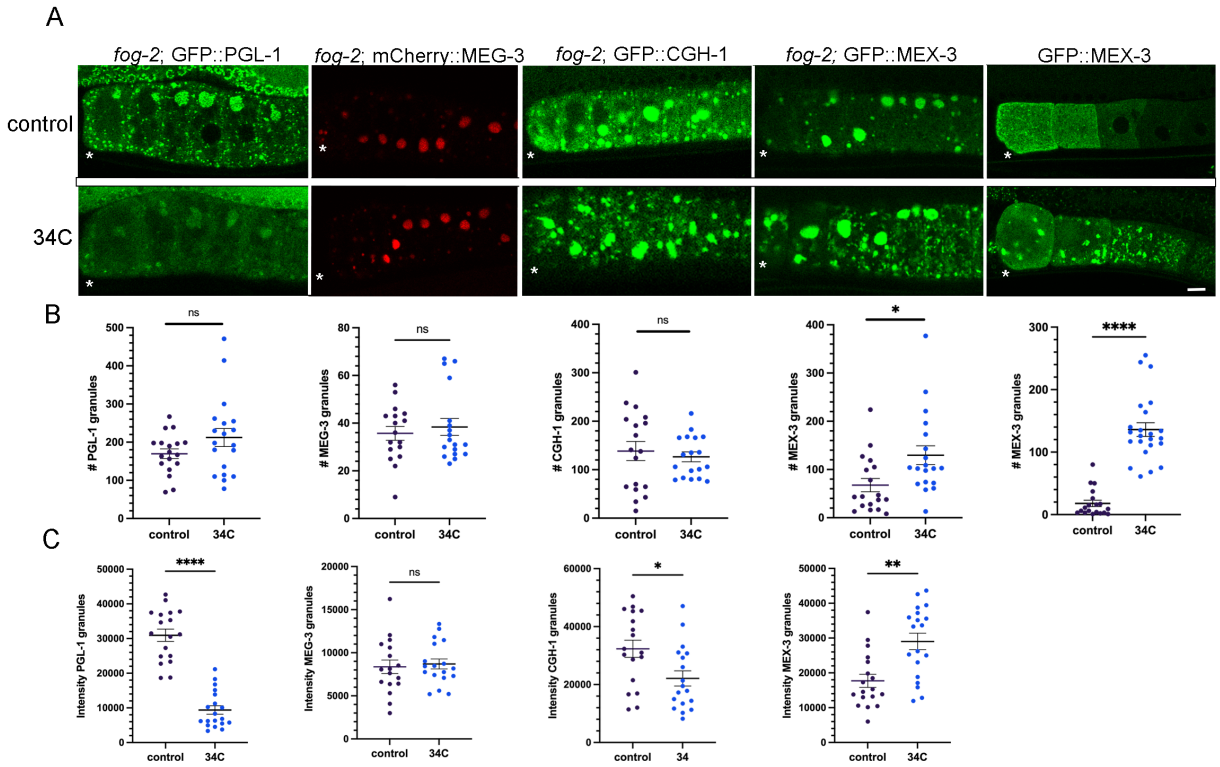

Figure 5. Increased temperature induces opposite phase transitions of RNA binding proteins. (A) Micrographs of three GFP-tagged RNA binding proteins in a *fog-2* background and GFP::MEX-3 in diakinesis oocytes. Top row: Distribution of GFP in control arrested oocytes at 20°C. Bottom row: Distribution of GFP in arrested oocytes after 40 min. at 34°C. Asterisk marks the most proximal oocyte in each germ line. Scale bar is 10 μm. (B) Graphs showing the number of GFP granules in a single Z-slice of proximal oocytes (see Methods). For B and C, statistical significance was determined using the Mann-Whitney test. **** indicates $p<0.0001$, ** indicates $p<0.01$, * indicates $p<0.05$, ns indicates not significant. n=17-23. Error bars indicate mean ±SEM. (C) Graphs showing the total intensity of GFP within granules in proximal oocytes (see Methods).

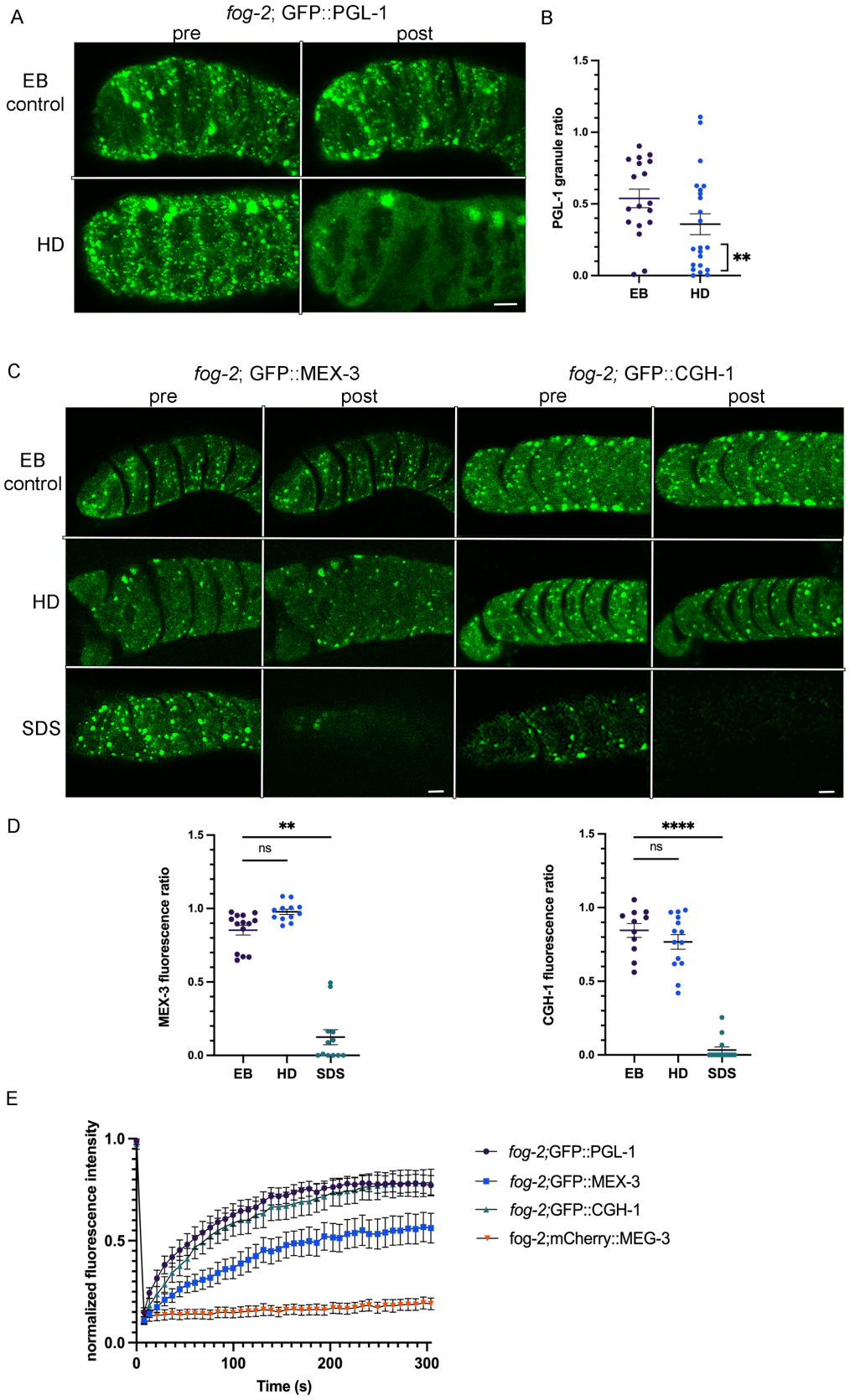
A
fog-2; GFP::PGL-1
pre
post
EB
control
HD
B
PGL-1 granule ratio
1.5
1.0
0.5
0.0
**
EB
HD
C
fog-2; GFP::MEX-3
fog-2; GFP::CGH-1
pre
post
pre
post
EB
control
HD
SDS
D
MEX-3 fluorescence ratio
**
ns
EB
HD
SDS
CGH-1 fluorescence ratio
****
ns
EB
HD
SDS
E
normalized fluorescence intensity
Time (s)
0
100
200
300
fog-2;GFP::PGL-1
fog-2;GFP::MEX-3
fog-2;GFP::CGH-1
fog-2;mCherry::MEG-3

Figure 6. PGL-1 is a liquid-like phase within large RNP granules in arrested oocytes. (A) Micrographs of *fog-2*; GFP::PGL-1 oocytes pre- and post-treatment with egg buffer (EB) control or 5% hexanediol (HD). Proximal oocytes are oriented to the left. Scale bar is 10 μm. (B) Graph showing the ratio of number of GFP::PGL granules pre- and post-treatments. Statistical significance was determined using the Fisher Exact test. ** indicates $p<0.01$. n=18-22. (C) Micrographs of *fog-2*; GFP::MEX-3 and *fog-2*; GFP::CGH-1 oocytes pre- and post-treatment with egg buffer (EB) control, 5% hexanediol (HD), or 10% SDS. Scale bar is 10 μm. (D) Graphs showing the ratio of total intensity of GFP in granules, pre- and post-treatments. Statistical significance was determined using the Kruskal-Wallis test. ** indicates $p<0.01$, ns indicates not significant. n=11-14. (E) FRAP of GFP::PGL-1, GFP::CGH-1, GFP::MEX-3 and GFP::MEG-3 in arrested oocytes of *fog-2* females. An area of 3.68μm^2 was bleached within a large granule. Granule intensity was measured every 7.8 seconds during a recovery phase of 300 seconds after photobleaching. Values were normalized to a reference granule intensity and plotted as an average of multiple experiments. n=8-12. Error bars are mean ±SEM.

ACKNOWLEDGEMENTS

We appreciate strains provided by Dr. Pam Padilla, Dr. Dustin Updike, Dr. Geraldine Seydoux, and the *Caenorhabditis* Genetics Center, which is funded by NIH Office of Research Infrastructure Programs (P40 OD010440). We thank Wormbase. C.P. was supported by an Undergraduate Summer Scholars grant from the Office of Research and Graduate Studies at Central Michigan University. Funding for this work came from a CMU Faculty Research and Creative Endeavors grant to J.S. and the NIH, grant 2R15GM109337-02A1 to J.S.

References

Aghayeva U, Bhattacharya A, Hobert O. 2020. A panel of fluorophore-tagged daf-16 alleles. MicroPubl Biol. 2020. doi:10.17912/micropub.biology.000210. https://www.ncbi.nlm.nih.gov/pubmed/32550509.

Alberti S, Carra S. 2018. Quality Control of Membraneless Organelles. J Mol Biol. 430(23):4711–4729. doi:10.1016/j.jmb.2018.05.013. https://www.ncbi.nlm.nih.gov/pubmed/29758260.

An JH, Blackwell TK. 2003. SKN-1 links C. elegans mesendodermal specification to a conserved oxidative stress response. Genes Dev. 17(15):1882–1893. doi:10.1101/gad.1107803. https://www.ncbi.nlm.nih.gov/pubmed/12869585.

Banani SF, Lee HO, Hyman AA, Rosen MK. 2017. Biomolecular condensates: organizers of cellular biochemistry. Nat Rev Mol Cell Biol. 18(5):285–298. doi:10.1038/nrm.2017.7. https://www.ncbi.nlm.nih.gov/pubmed/28225081.
Billi AC, Alessi AF, Khivansara V, Han T, Freeberg M, Mitani S, Kim JK. 2012. The Caenorhabditis elegans HEN1 ortholog, HENN-1, methylates and stabilizes select subclasses of germline small RNAs. PLoS Genet. 8(4):e1002617. doi:10.1371/journal.pgen.1002617. https://www.ncbi.nlm.nih.gov/pubmed/22548001.
Bischof LJ, Kao CY, Los FC, Gonzalez MR, Shen Z, Briggs SP, van der Goot FG, Aroian R V. 2008. Activation of the unfolded protein response is required for defenses against bacterial pore-forming toxin in vivo. PLoS Pathog. 4(10):e1000176. doi:10.1371/journal.ppat.1000176. https://www.ncbi.nlm.nih.gov/pubmed/18846208.
Boag PR, Nakamura A, Blackwell TK. 2005. A conserved RNA-protein complex component involved in physiological germline apoptosis regulation in C. elegans. Development. 132(22):4975–4986. doi:10.1242/dev.02060. https://www.ncbi.nlm.nih.gov/pubmed/16221731.
Boke E, Ruer M, Wuhr M, Coughlin M, Lemaitre R, Gygi SP, Alberti S, Drechsel D, Hyman AA, Mitchison TJ. 2016. Amyloid-like Self-Assembly of a Cellular Compartment. Cell. 166(3):637–650. doi:10.1016/j.cell.2016.06.051. https://www.ncbi.nlm.nih.gov/pubmed/27471966.
Brenner S. 1974. The genetics of Caenorhabditis elegans. Genetics. 77(1):71–94. doi:10.1093/genetics/77.1.71. https://www.ncbi.nlm.nih.gov/pubmed/4366476.
Buijsen RA, Visser JA, Kramer P, Severijnen EA, Gearing M, Charlet-Berguerand N, Sherman SL, Berman RF, Willemsen R, Hukema RK. 2016. Presence of inclusions positive for polyglycine containing protein, FMRpolyG, indicates that repeat-associated non-AUG translation plays a role in fragile X-associated primary ovarian insufficiency. Hum Reprod. 31(1):158–168. doi:10.1093/humrep/dev280. https://www.ncbi.nlm.nih.gov/pubmed/26537920.
Corbet GA, Parker R. 2019. RNP Granule Formation: Lessons from P-Bodies and Stress Granules. Cold Spring Harb Symp Quant Biol. 84:203–215. doi:10.1101/sqb.2019.84.040329. https://www.ncbi.nlm.nih.gov/pubmed/32482896.
Draper BW, Mello CC, Bowerman B, Hardin J, Priess JR. 1996. MEX-3 is a KH domain protein that regulates blastomere identity in early C. elegans embryos. Cell. 87(2):205–216. doi:10.1016/s0092-8674(00)81339-2. https://www.ncbi.nlm.nih.gov/pubmed/8861905.
Duster R, Kaltheuner IH, Schmitz M, Geyer M. 2021. 1,6-Hexanediol, commonly used to dissolve liquid-liquid phase separated condensates, directly impairs kinase and phosphatase activities. J Biol Chem. 296:100260. doi:10.1016/j.jbc.2021.100260. https://www.ncbi.nlm.nih.gov/pubmed/33814344.
Fajner V, Giavazzi F, Sala S, Oldani A, Martini E, Napoletano F, Parazzoli D, Cesare G, Cerbino R, Maspero E, et al. 2021. Hecw controls oogenesis and neuronal homeostasis by promoting the liquid state of ribonucleoprotein particles. Nat Commun. 12(1):5488. doi:10.1038/s41467-021-25809-8. https://www.ncbi.nlm.nih.gov/pubmed/34531401.
Friedman-Gohas M, Elizur SE, Dratviman-Storobinsky O, Aizer A, Haas J, Raanani H, Orvieto R, Cohen Y. 2020. FMRpolyG accumulates in FMR1 premutation granulosa cells. J Ovarian Res. 13(1):22. doi:10.1186/s13048-020-00623-w.

https://www.ncbi.nlm.nih.gov/pubmed/32101156.
Fritsch AW, Diaz-Delgadillo AF, Adame-Arana O, Hoege C, Mittasch M, Kreysing M, Leaver M, Hyman AA, Julicher F, Weber CA. 2021. Local thermodynamics govern formation and dissolution of Caenorhabditis elegans P granule condensates. Proc Natl Acad Sci U S A. 118(37). doi:10.1073/pnas.2102772118. https://www.ncbi.nlm.nih.gov/pubmed/34507991.
Fuentes R, Mullins MC, Fernandez J. 2018. Formation and dynamics of cytoplasmic domains and their genetic regulation during the zebrafish oocyte-to-embryo transition. Mech Dev. 154:259–269. doi:10.1016/j.mod.2018.08.001. https://www.ncbi.nlm.nih.gov/pubmed/30077623.
Ganion LR. 1991. Cytoplasmic distribution of poly(A)-containing RNA in developing Necturus maculosus oocytes with reference to annulate lamellae. Anat Rec. 230(2):218–224. doi:10.1002/ar.1092300209 [doi].
Hanazawa M, Yonetani M, Sugimoto A. 2011. PGL proteins self associate and bind RNPs to mediate germ granule assembly in C. elegans. J Cell Biol. 192(6):929–937. doi:10.1083/jcb.201010106. https://www.ncbi.nlm.nih.gov/pubmed/21402787.
Henderson ST, Bonafe M, Johnson TE. 2006. daf-16 protects the nematode Caenorhabditis elegans during food deprivation. J Gerontol A Biol Sci Med Sci. 61(5):444–460. doi:10.1093/gerona/61.5.444. https://www.ncbi.nlm.nih.gov/pubmed/16720740.
Hubstenberger A, Noble SL, Cameron C, Evans TC. 2013. Translation repressors, an RNA helicase, and developmental cues control RNP phase transitions during early development. Dev Cell. 27(2):161–173. doi:10.1016/j.devcel.2013.09.024. https://www.ncbi.nlm.nih.gov/pubmed/24176641.
Jud MC, Czerwinski MJ, Wood MP, Young RA, Gallo CM, Bickel JS, Petty EL, Mason JM, Little BA, Padilla PA, et al. 2008. Large P body-like RNPs form in C. elegans oocytes in response to arrested ovulation, heat shock, osmotic stress, and anoxia and are regulated by the major sperm protein pathway. Dev Biol. 318(1):38–51. doi:S0012-1606(08)00188-7 [pii]10.1016/j.ydbio.2008.02.059 [doi].
Kapulkin WJ, Hiester BG, Link CD. 2005. Compensatory regulation among ER chaperones in C. elegans. FEBS Lett. 579(14):3063–3068. doi:10.1016/j.febslet.2005.04.062. https://www.ncbi.nlm.nih.gov/pubmed/15907843.
Kawasaki I, Amiri A, Fan Y, Meyer N, Dunkelbarger S, Motohashi T, Karashima T, Bossinger O, Strome S. 2004. The PGL family proteins associate with germ granules and function redundantly in Caenorhabditis elegans germline development. Genetics. 167(2):645–661. doi:10.1534/genetics.103.023093 [doi]167/2/645 [pii].
Lin Y, Mori E, Kato M, Xiang S, Wu L, Kwon I, McKnight SL. 2016. Toxic PR Poly-Dipeptides Encoded by the C9orf72 Repeat Expansion Target LC Domain Polymers. Cell. 167(3):789-802 e12. doi:10.1016/j.cell.2016.10.003. https://www.ncbi.nlm.nih.gov/pubmed/27768897.
Link CD, Cypser JR, Johnson CJ, Johnson TE. 1999. Direct observation of stress response in Caenorhabditis elegans using a reporter transgene. Cell Stress Chaperones. 4(4):235–242. doi:10.1379/1466-1268(1999)004<0235:doosri>2.3.co;2. https://www.ncbi.nlm.nih.gov/pubmed/10590837.
Little SC, Sinsimer KS, Lee JJ, Wieschaus EF, Gavis ER. 2015. Independent and coordinate trafficking of single Drosophila germ plasm mRNAs. Nat Cell Biol.

17(5):558–568. doi:10.1038/ncb3143. https://www.ncbi.nlm.nih.gov/pubmed/25848747.
Manjarrez JR, Mailler R. 2020. Stress and timing associated with Caenorhabditis elegans immobilization methods. Heliyon. 6(7):e04263. doi:10.1016/j.heliyon.2020.e04263. https://www.ncbi.nlm.nih.gov/pubmed/32671240.
McCarter J, Bartlett B, Dang T, Schedl T. 1999a. On the control of oocyte meiotic maturation and ovulation in Caenorhabditis elegans. Dev Biol. 205(1):111–128. doi:10.1006/dbio.1998.9109. https://www.ncbi.nlm.nih.gov/pubmed/9882501.
McCarter J, Bartlett B, Dang T, Schedl T. 1999b. On the control of oocyte meiotic maturation and ovulation in Caenorhabditis elegans. Dev Biol. 205(1):111–128. doi:S0012-1606(98)99109-6 [pii]10.1006/dbio.1998.9109 [doi].
Navarro RE, Shim EY, Kohara Y, Singson A, Blackwell TK. 2001. cgh-1, a conserved predicted RNA helicase required for gametogenesis and protection from physiological germline apoptosis in C. elegans. Development. 128(17):3221–3232. https://www.ncbi.nlm.nih.gov/pubmed/11546739.
Noble SL, Allen BL, Goh LK, Nordick K, Evans TC. 2008. Maternal mRNAs are regulated by diverse P body-related mRNP granules during early Caenorhabditis elegans development. J Cell Biol. 182(3):559–572. doi:jcb.200802128 [pii]10.1083/jcb.200802128 [doi].
Oh SW, Mukhopadhyay A, Svrzikapa N, Jiang F, Davis RJ, Tissenbaum HA. 2005. JNK regulates lifespan in Caenorhabditis elegans by modulating nuclear translocation of forkhead transcription factor/DAF-16. Proc Natl Acad Sci U S A. 102(12):4494–4499. doi:10.1073/pnas.0500749102. https://www.ncbi.nlm.nih.gov/pubmed/15767565.
Patel SS, Belmont BJ, Sante JM, Rexach MF. 2007. Natively unfolded nucleoporins gate protein diffusion across the nuclear pore complex. Cell. 129(1):83–96. doi:10.1016/j.cell.2007.01.044. https://www.ncbi.nlm.nih.gov/pubmed/17418788.
Pek JW, Anand A, Kai T. 2012. Tudor domain proteins in development. Development. 139(13):2255–2266. doi:10.1242/dev.073304. https://www.ncbi.nlm.nih.gov/pubmed/22669818.
Putnam A, Cassani M, Smith J, Seydoux G. 2019. A gel phase promotes condensation of liquid P granules in Caenorhabditis elegans embryos. Nat Struct Mol Biol. 26(3):220–226. doi:10.1038/s41594-019-0193-2. https://www.ncbi.nlm.nih.gov/pubmed/30833787.
Roovers EF, Kaaij LJT, Redl S, Bronkhorst AW, Wiebrands K, de Jesus Domingues AM, Huang HY, Han CT, Riemer S, Dosch R, et al. 2018. Tdrd6a Regulates the Aggregation of Buc into Functional Subcellular Compartments that Drive Germ Cell Specification. Dev Cell. 46(3):285-301 e9. doi:10.1016/j.devcel.2018.07.009. https://www.ncbi.nlm.nih.gov/pubmed/30086300.
Saha S, Weber CA, Nousch M, Adame-Arana O, Hoege C, Hein MY, Osborne-Nishimura E, Mahamid J, Jahnel M, Jawerth L, et al. 2016. Polar Positioning of Phase-Separated Liquid Compartments in Cells Regulated by an mRNA Competition Mechanism. Cell. 166(6):1572-1584 e16. doi:10.1016/j.cell.2016.08.006. https://www.ncbi.nlm.nih.gov/pubmed/27594427.
Schisa JA. 2012. New insights into the regulation of RNP granule assembly in oocytes. Int Rev Cell Mol Biol. 295:233–289. doi:10.1016/B978-0-12-394306-4.00013-7. https://www.ncbi.nlm.nih.gov/pubmed/22449492.

Schisa JA. 2019. Germ Cell Responses to Stress: The Role of RNP Granules. Front Cell Dev Biol. 7:220. doi:10.3389/fcell.2019.00220. https://www.ncbi.nlm.nih.gov/pubmed/31632971.
Schisa JA, Pitt JN, Priess JR. 2001. Analysis of RNA associated with P granules in germ cells of C. elegans adults. Development. 128(8):1287–1298.
Shen X, Ellis RE, Lee K, Liu CY, Yang K, Solomon A, Yoshida H, Morimoto R, Kurnit DM, Mori K, et al. 2001. Complementary signaling pathways regulate the unfolded protein response and are required for C. elegans development. Cell. 107(7):893–903. doi:10.1016/s0092-8674(01)00612-2. https://www.ncbi.nlm.nih.gov/pubmed/11779465.
Shimada Y, Burn KM, Niwa R, Cooley L. 2011. Reversible response of protein localization and microtubule organization to nutrient stress during Drosophila early oogenesis. Dev Biol. 355(2):250–262. doi:10.1016/j.ydbio.2011.04.022. https://www.ncbi.nlm.nih.gov/pubmed/21570389.
Snee MJ, Macdonald PM. 2009. Dynamic organization and plasticity of sponge bodies. Dev Dyn. 238(4):918–930. doi:10.1002/dvdy.21914. https://www.ncbi.nlm.nih.gov/pubmed/19301391.
Spike C, Meyer N, Racen E, Orsborn A, Kirchner J, Kuznicki K, Yee C, Bennett K, Strome S. 2008. Genetic analysis of the Caenorhabditis elegans GLH family of P-granule proteins. Genetics. 178(4):1973–1987. doi:10.1534/genetics.107.083469. https://www.ncbi.nlm.nih.gov/pubmed/18430929.
Strayer A, Wu Z, Christen Y, Link CD, Luo Y. 2003. Expression of the small heat-shock protein Hsp16-2 in Caenorhabditis elegans is suppressed by Ginkgo biloba extract EGb 761. FASEB J. 17(15):2305–2307. doi:10.1096/fj.03-0376fje. https://www.ncbi.nlm.nih.gov/pubmed/14525938.
Strome S, Wood WB. 1982. Immunofluorescence visualization of germ-line-specific cytoplasmic granules in embryos, larvae, and adults of Caenorhabditis elegans. Proc Natl Acad Sci U S A. 79(5):1558–1562.
Sundby AE, Molnar RI, Claycomb JM. 2021. Connecting the Dots: Linking Caenorhabditis elegans Small RNA Pathways and Germ Granules. Trends Cell Biol. 31(5):387–401. doi:10.1016/j.tcb.2020.12.012. https://www.ncbi.nlm.nih.gov/pubmed/33526340.
Trcek T, Grosch M, York A, Shroff H, Lionnet T, Lehmann R. 2015. Drosophila germ granules are structured and contain homotypic mRNA clusters. Nat Commun. 6:7962. doi:10.1038/ncomms8962. https://www.ncbi.nlm.nih.gov/pubmed/26242323.
Trcek T, Lehmann R. 2019. Germ granules in Drosophila. Traffic. 20(9):650–660. doi:10.1111/tra.12674. https://www.ncbi.nlm.nih.gov/pubmed/31218815.
Updike DL, Hachey SJ, Kreher J, Strome S. 2011. P granules extend the nuclear pore complex environment in the C. elegans germ line. J Cell Biol. 192(6):939–948. doi:10.1083/jcb.201010104. https://www.ncbi.nlm.nih.gov/pubmed/21402789.
Updike DL, Knutson AK, Egelhofer TA, Campbell AC, Strome S. 2014. Germ-granule components prevent somatic development in the C. elegans germline. Curr Biol. 24(9):970–975. doi:10.1016/j.cub.2014.03.015. https://www.ncbi.nlm.nih.gov/pubmed/24746798.
Walter P, Ron D. 2011. The unfolded protein response: from stress pathway to homeostatic regulation. Science (80-). 334(6059):1081–1086.

doi:10.1126/science.1209038. https://www.ncbi.nlm.nih.gov/pubmed/22116877.
Wang J, Robida-Stubbs S, Tullet JM, Rual JF, Vidal M, Blackwell TK. 2010. RNAi screening implicates a SKN-1-dependent transcriptional response in stress resistance and longevity deriving from translation inhibition. PLoS Genet. 6(8). doi:10.1371/journal.pgen.1001048. https://www.ncbi.nlm.nih.gov/pubmed/20700440.
Wang JT, Smith J, Chen BC, Schmidt H, Rasoloson D, Paix A, Lambrus BG, Calidas D, Betzig E, Seydoux G. 2014. Regulation of RNA granule dynamics by phosphorylation of serine-rich, intrinsically disordered proteins in C. elegans. Elife. 3:e04591. doi:10.7554/eLife.04591. https://www.ncbi.nlm.nih.gov/pubmed/25535836.
Watkins B, Schisa JA. 2021. Phase separation dynamics of the C. elegans PGL-1 P granule protein in oocytes are sensitive to heat stress. MicroPubl Biol. 2021. doi:10.17912/micropub.biology.000476. https://www.ncbi.nlm.nih.gov/pubmed/34585104.
Weber SC, Brangwynne CP. 2012. Getting RNA and protein in phase. Cell. 149(6):1188–1191. doi:10.1016/j.cell.2012.05.022. https://www.ncbi.nlm.nih.gov/pubmed/22682242.
Zhang H, Chang JT, Guo B, Hansen M, Jia K, Kovacs AL, Kumsta C, Lapierre LR, Legouis R, Lin L, et al. 2015. Guidelines for monitoring autophagy in Caenorhabditis elegans. Autophagy. 11(1):9–27. doi:10.1080/15548627.2014.1003478. https://www.ncbi.nlm.nih.gov/pubmed/25569839.